Characterization of Mixing and Size Segregation in a Rotating Drum by a Particle Tracking Method

Ebrahim Alizadeh, Olivier Dubé, François Bertrand, and Jamal Chaouki
Dept. of Chemical Engineering, École Polytechnique de Montréal, Montréal, Québec, Canada H3C 3A7

DOI 10.1002/aic.13982
Published online January 4, 2013 in Wiley Online Library (wileyonlinelibrary.com)

The mechanisms of segregation in solids mixing, even in simple rotating drums, are not clearly understood. Although most past studies have focused on binary mixtures, this work investigates the effect of polydispersity on granular flow, mixing, and segregation in a rotating drum operated in rolling regime through particle trajectories obtained from the radioactive particle tracking technique. Velocity profiles, radial segregation, and axial dispersion coefficients for monodisperse and polydisperse systems of glass beads are analyzed with respect to rotational speed and particle size. A model is introduced to predict the residence times along streamlines and evaluate the rate at which the material renews at the free surface and within the inner layers of the bed. Our results reveal similar velocity profiles and residence times for monodisperse and polydisperse systems. They also indicate that the particles distribute along the radial direction of the drum, although not necessarily in a core/shell configuration. © 2013 American Institute of Chemical Engineers
AIChE J, 59: 1894–1905, 2013
Keywords: solid mixing, segregation, rotating drum, radioactive particle tracking, velocity profile, residence time, axial dispersion

Introduction

Particulate materials are present in many industries, including ceramic, metallurgical, chemical, food, cosmetics, coal, plastics, and pharmaceutical. In some of them, it is preferable to separate species of a mixture, whereas in many others, the final product is obtained by mixing the ingredients so that their final concentrations meet specific requirements within a given level of scrutiny. Blenders are commonly used in such industries to obtain a homogeneous mixture. Despite the wide applications reported for these blenders, their mechanisms of mixing are still poorly understood,[1] so much that the dynamics of granular materials was identified as one of the 125 questions (Can we develop a general theory of the dynamics of turbulent flows and the motion of granular materials?) that point to critical knowledge gaps in science.[2] In fact, during the last few decades, a large body of work has focused on the flow of granules and powders. However, more investigations are needed. Here, we restrict ourselves to the simple rotating drum, which is used, for instance, as a granular mixer, a dryer, a coater, or a gas/solid reactor. In the rotating drum, different types of flow regimes are obtained by increasing the Froude number, $Fr = \frac{\omega^2 R}{g}$, where ω, R, and g stand for the rotational speed, the drum radius, and the gravitational acceleration, respectively.[3,4] In this article, we focus on the rolling regime that is common for mixing purposes. It is characterized by a flat surface layer, where the particles flow at a given dynamic repose angle with respect to the horizontal. This dynamic repose angle depends on granule properties such as size and surface roughness, as well as on the tumbler dimensions and rotational speed.[3]

As shown in Figure 1, the granular bed in the rolling mode can be divided into two distinct regions: (1) a thin lens-like flowing or active layer and (2) a larger passive layer beneath the active layer. In the passive region, the particles flow as a solid body and rotate with the drum at fixed axial and radial positions. When particles reach the surface, they slide down within the active layer and eventually rejoin the passive layer.

One of the phenomena that makes mixing of granules difficult is segregation (demixing). In mixers, segregation happens when particles have different properties, such as size, density, shape, and roughness. Although segregation occurs in tumbling blenders, its mechanisms are not clearly understood and all known theories or explanations have exceptions. Segregation can happen in both radial (transverse) and axial directions in a tumbling drum. As the radial mixing mechanism is mainly convective, radial segregation appears rapidly in the first few revolutions.[5] Depending on the particle-size distribution and the fraction of large particles, fine and dense particles generally migrate to the core region of the material bed near the rotation axis.[5–8] As the particle axial and radial positions do not change in the passive layer owing to the solid-like motion, segregation starts in the active layer near the free surface and only a very slow rearrangement of the particles occurs below this flowing layer.[9,10] Segregation in the transverse plane (that parallel to the drum ends) mainly results from the downward movement of small (or dense) particles within a thin surface layer,

Correspondence concerning this article should be addressed to F. Bertrand at francois.bertrand@polymtl.ca or J. Chaouki at jamal.chaouki@polymtl.ca.

© 2013 American Institute of Chemical Engineers

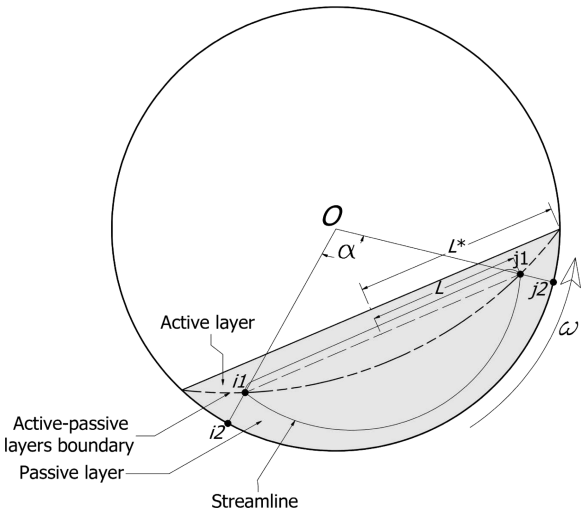

Figure 1. Rolling regime in a cylindrical drum.

which displace larger (or lighter) particles upward.[3] After a long enough period of the time, axial bands of coarse and fine particles are often formed. These bands are generally rich in one type of particles, but not necessarily pure. Axial banding segregation has been the topic of numerical and experimental works.[6,10–15] In particular, Hill and Kakalios[15] showed that blends that appear mixed at low rotational speed may form bands at higher speed. The governing mechanism for such axial segregation is not clear. However, it has been shown that differences in the dynamic repose angle of the components of a blend may trigger the formation of these axial bands.[15,16] Recently, Chen et al.[17] showed the effect of the end walls of the cylindrical drum on axial segregation. As the governing mixing mechanism in the axial direction is dispersion, axial segregation occurs more slowly than radial segregation and may require hundreds or even thousands of revolutions.

In the studies mentioned earlier, binary mixtures of granules were considered. In fact, investigations on the flow of polydisperse blends are rare, one example being the work of Ingram et al.[18] Therefore, it is of interest to investigate the effect on granular flow of a distribution of particle sizes inside the bed. This would help to find out whether theories and correlations that have been developed for monodisperse, and binary mixtures are valid for more complex polydisperse systems.

The aim of this study is to gain insight into the flow dynamics of polydisperse particles in a cylindrical drum as well as the underlying mixing and segregation mechanisms. Parameters such as the residence time, active layer thickness, and axial dispersion are discussed in detail. Understanding of these parameters is important, as it may provide guidelines for the design of efficient mixing processes and other unit operations involving particles. In this work, only free flowing particles are considered, so that noncontact forces such as cohesive forces are neglected. Radioactive particle tracking (RPT), which was used to capture the flow of particles inside the rotating drum, is described in next section. These RPT experiments differ from previous studies, because the tracers used and the particles in the drum have identical properties. The methodology and RPT experiments are then fully described, and the results obtained are presented thoroughly discussed.

Methodology

Characterizing the flow and the arrangement of the particles inside the drum can be done by extracting samples from it. However, such methods interfere with the matter and may affect the measurement itself.[19,20] In addition, analyzing samples containing many species is tedious and takes a long time. To overcome these limitations, noninvasive methods such as laser Doppler anemometry and particle image velocimetry are appealing at first sight, but the opaque nature of granular media renders such methods useless. Another possibility is to resort to characterization methods based on radioactive measurements. Two such methods have been applied in the field of solid mixing. The first one relies on positron annihilation and is called positron emission particle tracking (PEPT).[21,22] The second method, which is applied in this work, uses gamma rays emitted from a single radioactive tracer.[23] This technique is known as RPT and, in comparison with PEPT, is inexpensive, compact and can be used for large mixing vessels. Our group has extended RPT, so that it can be used in blenders.[24]

RPT

RPT tracks the position of a single radioactive tracer with respect to time using an array of scintillation detectors located around the vessel to capture gamma rays emitted by this tracer. The set of recorded gamma ray counts depends on the position of the tracer. The position of this tracer is in fact reconstructed by minimizing the discrepancy between the recorded and calculated counts using a model proposed by Beam et al.[25] This method uses Monte Carlo simulation to generate a dictionary that contains the number of gamma rays expected to be intercepted by the detectors when the tracer is in a given position. More details on this method can be found in Larachi et al.[23] and Doucet et al.[24] The RPT method has a resolution of 2–3 mm in all three directions (x, y, and z) under the conditions of this work.

RPT with ^{24}Na

One important step of the RPT method is the preparation of the tracer. In particular, this tracer should match the inert particles in size, density, and shape. One way to achieve this consists of radioactivating particles that are identical to those in the vessel. For instance, the glass beads used in this work contain 13–14% soda lime, which includes ^{23}Na that can be converted to ^{24}Na isotope using the Slowpoke reactor of École Polytechnique de Montréal. In practice, only one particle in the vessel is radioactive, the tracer, and the others are inert. The activation time of the tracers depends on their size and may vary from 30 to 90 min. ^{24}Na emits gamma rays with two levels of energy (1.368 and 2.754 MeV). In this study, only events related to the gamma rays with the higher energy are captured to prevent recording diffracted rays. The problem of ^{24}Na is its short half-life ($\sim$15 h). Depending on the duration of an experiment, the dictionaries that are valid at the beginning of such an experiment may then become inaccurate due to the decay of the ^{24}Na isotope, which may lead to large errors in the reconstruction of the tracer trajectory. To overcome this problem, recorded events must be corrected. To do so, a second tracer, which is similar to the first one, is used as a sentinel outside the vessel to monitor with the help of a dedicated NaI-Tl detector the loss of activity with time and then correct the number of events captured by the detectors around the vessel. Note that this

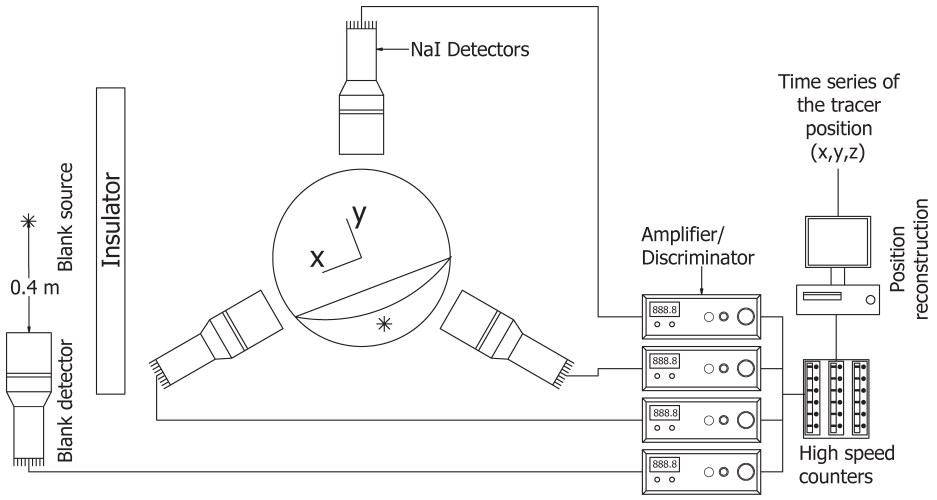

Figure 2. Schematic of the setup.

so-called blank source is shielded in such a way that it does not affect the measurements made by these detectors.

Experiments

Material

The RPT technique was applied to investigate flow behavior and mixing inside a horizontal rotating drum made from plexiglass. The drum has a 24-cm inner diameter and is 36-cm long. The drum was filled up to 35 vol % with glass beads (ρ = 2.5 kg/L) of varying diameter between 3 and 6 mm. The rotational speed of the drum was set to 11.6 RPM, which is the maximum velocity for the rolling mode. To study the effect of the rotational speed on the granular flow behavior, other sets of experiments were carried out at about 50% of the maximum rolling regime velocity (5.4 RPM). A schematic of the setup used for the experiments is given in Figure 2. Eight $3'' \times 3''$ NaI-Tl scintillation detectors were installed around the drum. Six detectors were strategically placed at 120° from each other around the drum, and two other detectors were positioned at both its ends. The distance between the detectors and the drum was fixed in such a way to avoid the saturation of gamma rays. The dwell time, let alone the time for each measurement by a detector, was set to 10 ms to minimize event fluctuations and track the tracer with adequate accuracy with respect to the maximum particle velocity inside the drum.

The approximate activity level was 60 μCi initially. To eliminate the effects of the other isotopes (e.g., antimony), which have a shorter half-life, the tracers were used 1–2 h after their activation in the Slowpoke reactor. The only change in the properties of a tracer after its activation was a darkening of its original color. The darker color of the tracer helps find it inside the bed after an experiment. Because chipping or erosion of the tracer may affect its properties as well as the RPT accuracy, the inner surface of the drum was checked for contamination with accurate germanium detectors after each experiment. It confirmed that the tracers did remain sealed, and their surface and physical properties remained identical to those of the other particles in the drum.

Details of the experiments

Mixing experiments were performed with 3-mm monodisperse glass beads and polydisperse mixtures of glass beads, the diameter of which were 3, 4, 5, or 6 mm. The composition of the polydisperse systems was chosen to ensure a rapid segregation in the drum (Table 1). Overall, 10 different experiments were performed. In each one, the radioactive tracer was tracked using RPT for a period of 210 min to make sure that it travels everywhere inside the drum. Details of the experiments are given in Table 1. The RPT data were then postprocessed to reconstruct the trajectory of the tracer.

Results

The RPT data can be exploited to gain insight into the flow behavior and mixing performance in the drum. First, velocity profiles on a transverse plane are presented. A model is then proposed to characterize the residence time of the glass beads in the active and passive layers, and its validity is assessed with experimental data. Finally, the radial segregation and the axial dispersion of the polydisperse mixtures with respect to the drum rotational speed and tracer size are analyzed.

Occupancy plots

As mentioned in the previous section, the particles retain their properties, when they are irradiated. This can also be assessed indirectly by checking that the occupancy plot of a tracer in a monodisperse system is homogenous, which means that it appears the same amount of time everywhere

Table 1. Mixing Experiments Involving Monodisperse and Polydisperse Particles

Case	Type	Rotational Speed (RPM)	Tracer Size (mm)
MD1	Monodisperse (3 mm)	5.4	3
MD2	Monodisperse (3 mm)	11.6	3
PD1.3	Polydisperse	5.4	3
PD1.4	(3mm(15vol%), 4mm(35vol%), 5mm(35vol%), 6mm(15vol%))	5.4	4
PD1.5		5.4	5
PD1.6		5.4	6
PD2.3	Polydisperse	11.6	3
PD2.4	(3mm(15vol%), 4mm(35vol%), 5mm(35vol%), 6mm(15vol%))	11.6	4
PD2.5		11.6	5
PD2.6		11.6	6

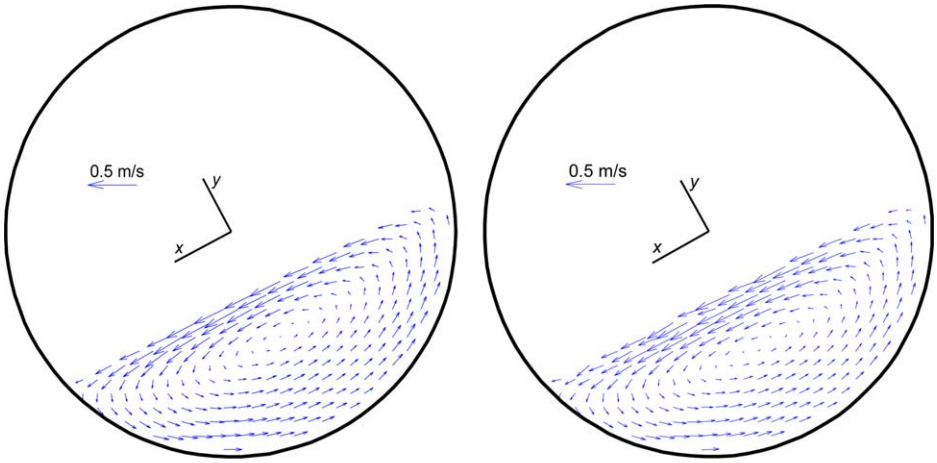

Figure 3. Velocity vectors in the transverse plane of the drum for (a) monodisperse (case MD2) and (b) polydisperse (case PD2) glass beads.

[Color figure can be viewed in the online issue, which is available at wileyonlinelibrary.com.]

in the volume of the drum and that no segregation, therefore, takes place. Obtaining occupancy plots using the RPT technique is straightforward, as this method collects large amounts of tracer positions during an experiment. These positions can be projected onto transverse planes of the drum to yield occupancy profiles (see Figure 8 for an example). Occupancy plots for monodisperse cases MD1 and MD2 indeed indicate (not shown here) that the tracer travels homogenously inside the drum.

Velocity profiles

The velocity of the tracer can be obtained by differentiating its position with respect to time. To obtain an average value of the velocity profile in a transverse plane, all of the reconstructed tracer positions and their corresponding velocities are projected onto it. Figure 3 shows typical velocity profiles in the transverse plane of the drum for cases MD2 (monodisperse) and PD2 (polydisperse). The velocity profile of the polydisperse mixture has been obtained by averaging the velocity profiles of all particles, irrespective of their sizes. Similar qualitative patterns can be observed for the monodisperse and polydisperse systems, and it seems a priori that the velocity profile is independent of the particle-size distribution.

A qualitative comparison of the monodisperse and polydisperse cases can be done by looking at the corresponding velocity profiles in the streamwise (x) and transverse (y) directions. Coordinate (0,0,0) is located at the center of the drum, x is parallel to the free surface in the direction of the flow, whereas y is perpendicular to the free surface and points outward. The z axis is aligned with the axial direction. Only the streamwise and transverse velocities for a rotational speed of 11.6 RPM are presented, as the results at the lower speed show the same trend. Figure 4 presents the transverse (v) and streamwise velocity (u) variations along the line at $x = 0$. These data were obtained by projecting the full data on the transverse plane of the drum by means of 2×2 mm^2 cells. On average, the tracer passes in each cell more than 400 times in each experiment, thus, providing statistically reliable data.

It is commonly assumed in the literature that there is no transverse velocity (v) at $x = 0$. Recently, Jain et al.[26] performed experiments with steel balls and showed that the transverse velocity varies slightly around zero. Our results show that the mean transverse velocity along the depth of the granular bed at $x = 0$ is -1.46×10^{-3} m/s (standard deviation $= 6.4 \times 10^{-3}$) and 2.2×10^{-3} m/s (standard deviation $= 6.9 \times 10^{-3}$) for the polydisperse and monodisperse cases, respectively. In the passive layer, the glass beads flow as a solid body, whereas in the active layer, these particles can slightly move in the y-direction.

As regards the streamwise velocity (u), one may observe that:

- Despite the occurrence of radial segregation for the polydisperse cases, as will be discussed later, there are no significant differences in the streamwise velocity profiles with respect to particle size;
- There are no significant differences between the velocity profiles of the polydisperse and monodisperse systems. The only small difference is that the velocity profile of the monodisperse mixture is slightly above those of the polydisperse mixtures, indicating a slightly thinner active layer in the former case;
- The streamwise velocity varies approximately linearly with respect to y in the active and passive layers, although with different slopes.

The linear behavior of the streamwise velocity is a well-known phenomenon and similar results, based on either numerical simulation or experimentation, have been reported in the literature.[3,12,27–29] Each of the two regions (active and passive) is characterized by a line and a slope. This behavior remains valid for other positions in x, as can be seen in Figure 5. The solid lines are the best fitted lines in the active layer for different positions in x, and the dashed line is what is expected in the passive layer and the solid body rotation found therein. The slope of the solid lines in the active layer increases with increasing x. When $x = 0$, the linear velocity profiles in the active and passive layers were obtained from the following correlations

$$u_{\mathrm{act}} = u_{\max}\left(1 + \frac{y+H}{\delta_\circ}\right) \tag{1}$$

$$u_{\mathrm{pas}} = \omega y \tag{2}$$

where $u_{\max}$ is the maximum value of the streamwise velocity on the free surface, H, the distance from the free surface to the center of the drum, and $\delta_\circ$, the distance from the surface

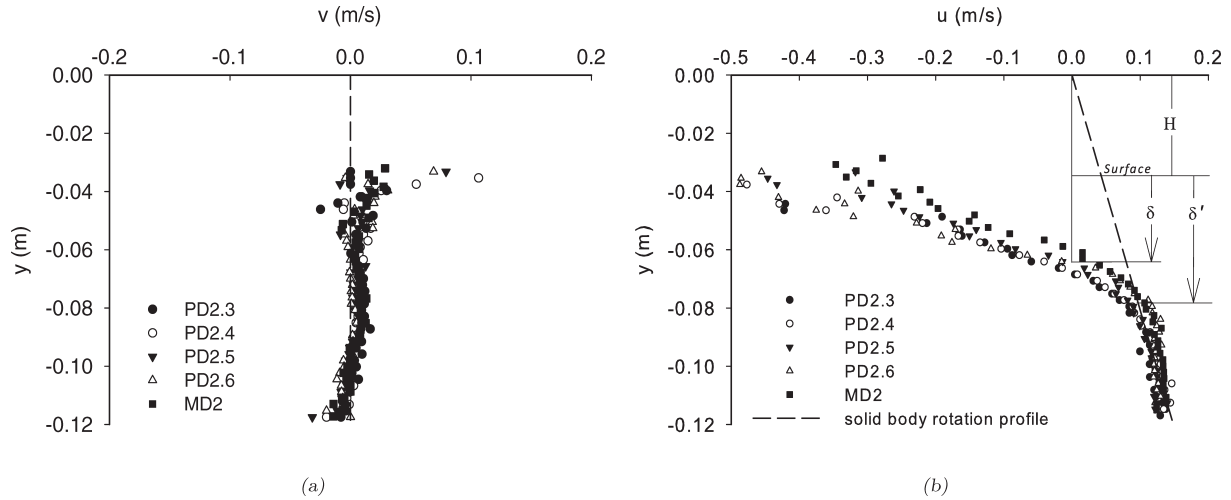

Figure 4. Variation of the (a) transverse and (b) streamwise velocities for a rotational speed of 11.6 RPM in the transverse plane of the drum along the line at $x = 0$.

***H* is the distance from the free surface to the center of the drum, δ is the distance from the free surface to the depth at which glass beads change direction along the *x* axis, and δ' is the distance from the free surface to the depth at which the solid body rotation stops.**

to the depth at which the glass beads change direction along the x axis, hereafter called the active layer thickness.

Another important aspect involves the variation of the streamwise velocity along the free surface. For example, Chen et al.[17] evidenced the effect of the surface flow on axial segregation. To show the surface flow, normalized velocities for the monodisperse and polydisperse cases were evaluated from the RPT data. The results are reported in Figure 6a. Note that, due to the probability of particles jumping off the surface, the data are shown a few millimeters beneath the top of the bed. The streamwise velocities were normalized with respect to the maximum value ($u_{\max}$) attained at the middle of the surface when $x = 0$. Along the free surface, the particles accelerate until they reach the middle point and then decelerate as they proceed toward the downstream endpoint. It can be shown that the particle velocity profile along the free surface can be expressed as[30]

$$\frac{u}{u_{\max}} = 1 - \frac{x^2}{L^{*2}} \tag{3}$$

$$u_{\max} = \omega L^{*2}/\delta_{\circ} \tag{4}$$

where $L^* = L|_{y=-H}$ corresponds to half the length of the free surface and, more generally, L corresponds to half the length of the corresponding streamline (see Figure 1). As illustrated in Figure 6a, the experimental data of the velocity profiles along the upstream half of the free surface can be adequately modeled by Eq. 3 (dashed curve). The downstream half is better approximated by a change in the exponent of Eq. 3 (solid curve), as has been reported by Ding et al.[31] It can also be seen that one single curve is needed to represent the streamwise velocity profile along the free surface for all monodisperse and polydisperse cases. The same model (with L^* replaced by L) can be applied for the streamlines in the inner layers of the bed. In this case, the velocity is normalized with respect to u_{act}, which is the maximum streamwise velocity evaluated from Eq. 1. Similar conclusions can be drawn, as can be seen in Figure 6b. Despite a slightly better fit of the solid curve in the downstream half of the graph of Figure 6b, the following expression, similar to Eq. 3, will be used in the rest of the article

$$u = u_{\text{act}}\left(1 - (x/L)^2\right) \tag{5}$$

Active layer thickness

The active layer thickness is an important parameter in models used for the material transport in rotating drums.[32] In fact, the thickness of the active layer has an impact on the mixing and segregation phenomena occurring in the drum. As a result, its determination is key to a better understanding of the kinetic and the extent of such phenomena. For instance, in a kiln operated in rolling regime, it has been shown that the thermal efficiency is proportional to the fraction of the mixing zone.[33] In direct-fired rotary kilns, the heat is mainly transferred into the bulk of the material bed through the active layer.[34]

The intersection point of the velocity profiles in the active and passive layers is known as the active layer lower

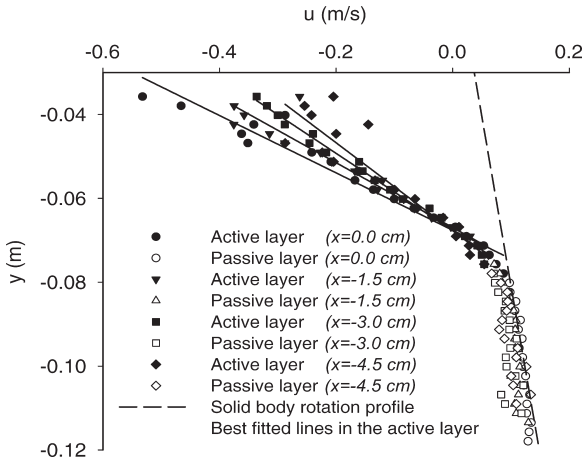

Figure 5. Streamwise velocity profiles for the polydisperse mixture of case PD2 for different positions in *x*.

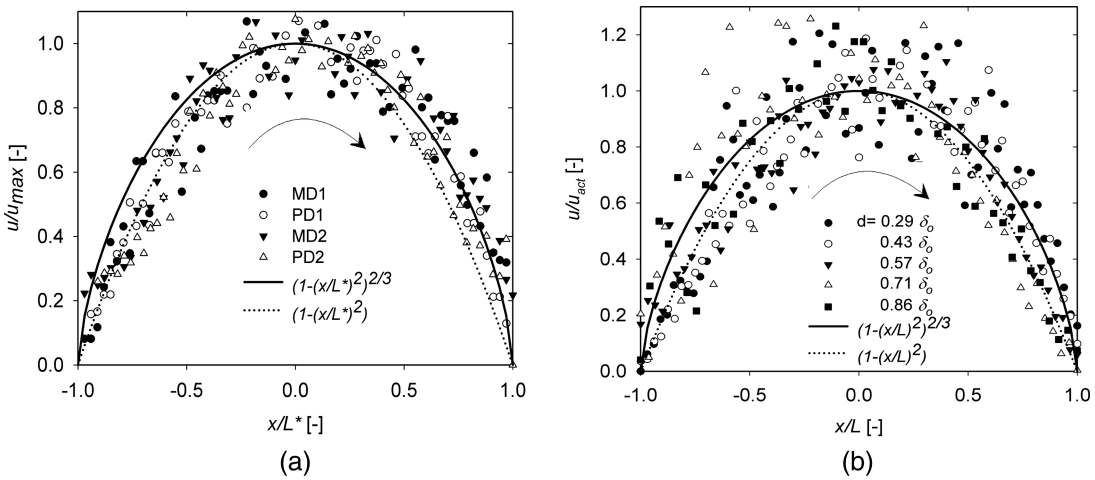

Figure 6. Streamwise velocity profiles along the *x*-direction; (a) on the free surface and (b) in the inner layers, in the case of MD2.

***d* stands for the distance from the free surface, $L = L(y)$ corresponds to half the length of the corresponding streamline in the active layer, and $L^* = L|_{y=-H}$. u_{act} is the velocity at the middle of each streamline.**

boundary where the particles stop rotating as a solid body and start free flowing. This is indicated by δ' in Figure 4b. In other studies, this boundary is defined as the point where the particles change direction ($u = 0$) along the x axis, as defined by δ in Figure 4b.[18] This second definition, called the "turning point criterion," is associated with a parabolic representation of the boundary

$$y = ax^2 - (H + \delta_o) \tag{6}$$

where $\delta_\circ = \delta|_{x=0}$. Parameter $a = \delta_\circ / L^{*2}$ is the parabolic constant, where $L^* = 11.5$ cm, the value of which depends on the fill level and the radius of the drum. The depth of the active layer at $x = 0$ (as expressed by $\delta'_\circ = \delta'|_{x=0}$ and $\delta_\circ$) for the different experiments is given in Tables 2 and 3. Note that PD1 and PD2 correspond to average values obtained for the four corresponding polydisperse cases. Contrary to the belief that the active layer is a rather thin layer, it can be around 30–40% of the total bed depth, based on these two definitions. As can be seen in the tables, the depth of the active layer is thicker for a polydisperse mixture and increases when the rotational speed is increased. This is in agreement with most of the data reported in the literature.[40–43]

Being able to evaluate the active layer thickness is important, because it affects the particle velocity profile. There are correlations in the literature that predict the thickness of the active layer as a function of x. Unfortunately, many of them include parameters (e.g., the maximum surface velocity) that are difficult to measure, mostly in industrial scale unit operations.[30] We propose here to resort to a model that predicts the depth of the active layer based only on the operating conditions, the material properties, and the geometrical characteristics of the rotating drum.[3,44,45] It is given by

$$\delta'(x) = \sqrt{\omega / \dot{\gamma}(L^{*2} - x^2)} \tag{7}$$

where the shear rate $\dot{\gamma}$ depends on the material properties

$$\dot{\gamma}(x) = \sqrt{\frac{g\cos\beta(x)\sin(\beta_d - \beta_s)}{d_p \cos\beta_d \cos\beta_s}} \tag{8}$$

with d_p the particle size and $\beta(x)$ the angle between the horizontal axis and the boundary between the active and passive layers. β_s and β_d are the measured static and dynamic angles of repose, which are equal to 25° and 27°, respectively. At $x = 0$, $\beta(0) \rightarrow \beta_d$ and the calculated values of $\delta'_\circ$ are given in Table 2. As can be seen, this model predicts accurately the thickness of the active layer except for the case PD1, where a reasonable 17% discrepancy is obtained.

Recently, Cheng et al.[35] applied an incomplete similarity theory for estimating $\delta_\circ$ when the drum was half filled. They extended their correlation to cover various fill fractions and fitted the underlying constants using experimental data of Felix et al.,[46,47] where glass beads have been used. Other expressions have been developed by Ding et al.,[36,37] Weir et al.,[39] and Liu et al.[34,38] As these models suffer from weak predictions or need fitting constants, in this work, a new correlation is proposed for $\delta_\circ$. Given that the linear streamwise velocity profiles in the active (Eq. 1) and passive (Eq. 2) layers meet at $y = -(\delta'_\circ + H)$ (see Figures 4 and 5), it follows that

$$u_{act}|_{y=-(\delta'_\circ + H)} = u_{pas}|_{y=-(\delta'_\circ + H)} \tag{9}$$

$$\delta_\circ = \frac{\delta'_\circ u_{max}}{u_{max} + \omega(H + \delta'_\circ)} \tag{10}$$

and, from Eq. 4

$$1 - \frac{L^{*2}}{\delta_o^2} \frac{\delta'_\circ - \delta_\circ}{H + \delta'_\circ} = 0 \tag{11}$$

The values of $\delta_\circ$ using Eq. 11 and those obtained with the correlations from the literature are presented in Table 3. A good agreement with the experimental data is obtained in all cases, when Eq. 11 is used. This shows the ability of this

Table 2. Depth of the Active Layer $\delta'_\circ$

Case	Type	ω (RPM)	$\delta'_\circ$ [Measured; cm (%)[a]]	$\delta'_\circ$ [Eq. 7; cm (%)[a]]
MD1	Monodisperse	5.4	2.6 (30)	2.6 (30)
MD2		11.6	3.8 (43)	3.8 (43)
PD1	Polydisperse	5.4	3.5 (40)	2.9 (33)
PD2		11.6	4.2 (48)	4.2 (48)

[a]Percentage of bed depth.

Table 3. Depth of the Turning Point Active Layer ($\delta_\circ$)

Case	ω (RPM)	Measured	Eq. 11	Cheng et al.[35]	Ding et al.[36,37]	Liu et al.[34,38]	Weir et al.[39]
MD1	5.4	2.1 (24)	2.4 (27)	1.9 (21)	2.5 (28)	1.5 (18)	2.1 (24)
MD2	11.6	2.8 (32)	3.3 (37)	2.1 (24)	2.3 (27)	2.0 (23)	2.6 (30)
PD1	5.4	2.6 (30)	2.6 (30)	1.8 (21)	3.0 (34)	1.6 (18)	2.4 (28)
PD2	11.6	2.9 (33)	3.5 (40)	1.7 (20)	2.8 (32)	2.1 (24)	3.0 (34)
Average error (%)		-	13	27	13	30	4

All data are in centimeter (percentage of bed depth).

expression to predict the active layer thickness, which can then be used to derive velocity profiles by means of Eqs. 1 and 4. Among the correlations from the literature, the one by Weir et al.[39] yields the best results. Their model predicts that $\delta_\circ$ increases with increasing particle size or rotational speed. However, it brings into play an author-dependent coefficient (λ), the value of which depends on particle properties, the geometrical characteristics of the drum and the operating conditions. They used $\lambda = 1$ for glass beads based on the experimental data of Felix et al.,[46] which was used in the last column of Table 3 to predict the value of $\delta_\circ$ with their expression. As the operating conditions in Felix et al.[46] are close to the conditions of the experiments of this work ($d_p < 2$ mm, $\omega = 2.0$-10.4 RPM, and $R = 0.06$–0.20 m), very small discrepancies are observed between the values predicted by this model and the measured values of $\delta_\circ$. However, a larger error could be obtained for operating conditions far from those considered to fit coefficient λ. The advantages of Eq. 11 comes from the fact that its parameters are easy to obtain: H and L^* from geometrical conditions and δ' using Eqs. 7 and 8. The predictions from the models of Liu et al.[34,38] and Cheng et al.[35] underestimate the thickness of the active layer, although the former does predict the behavior of $\delta_\circ$ when the rotational speed increases or the mixture changes from MD to PD. Finally, the model by Ding et al.[36,37] performs rather well as regards the thickness of active layer (average error of 13%) and succeeds to predict the behavior of $\delta_\circ$ when the type of mixture changes, but fails to correctly predict the trend when the rotational speed changes.

Residence time

In the cylindrical drum, the transverse motion of the particles is the primary factor that controls the renewal of the material at the exposed bed surface. In particular, the rate of surface renewal affects the heat/mass transfer from the freeboard to the bed.[48] For example, in industrial pan coaters, where a nozzle sprays the surface of the bed, the coating time is related to the residence (cycling) time of the granules on the free surface.[49] Another example is the granulation process with rotating drums, where the determination of the residence time in the different layers of the granular bed could help estimate local rates of granulation and then the granulation time. These facts have provided the impetus to model the residence time of the particles on the free surface as well as in the inner layers of the granular bed.

In Figure 7, the total residence time of the glass beads along streamlines (t_t), as evaluated from RPT data, is shown vs. the angle α of these streamlines (Figure 1) for the monodisperse and polydisperse cases. It corresponds to the time taken by these particles to make one full circulation along a closed streamline. As can be noticed, there is a linear increase in the residence time when the angle of the streamlines increases. To analyze these results in more detail, the residence time can be divided into two components corresponding to the active and passive layers. In the passive layer, because of the solid body motion, a linear increase of the residence time is expected when α increases. This can be shown for an arbitrary streamline that displaces particles from $i1 \rightarrow j1$ (see Figure 1). Due to the solid body rotation

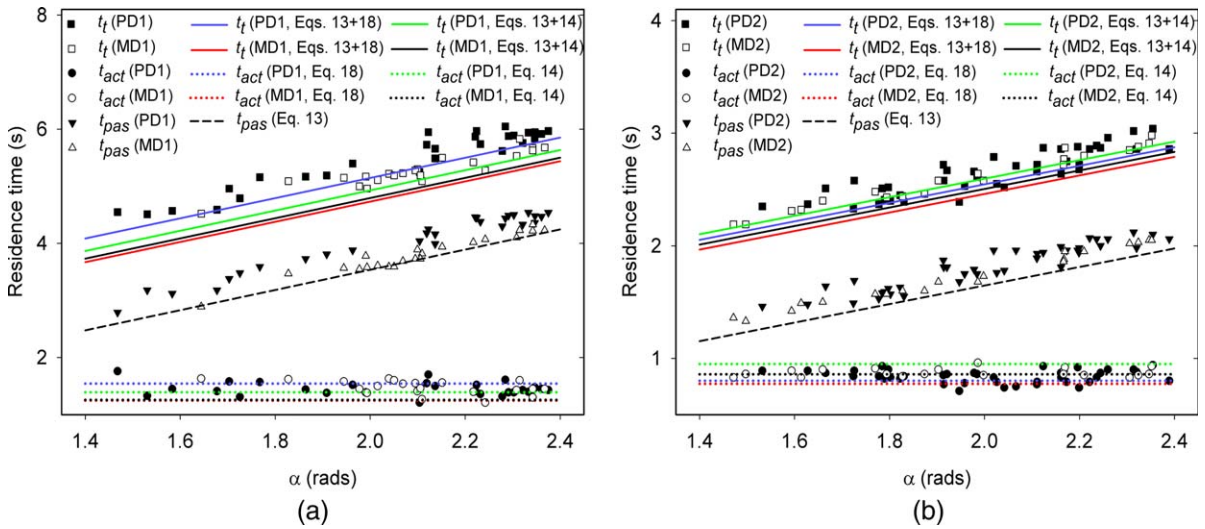

Figure 7. Variation of the residence time vs. the angle of the streamlines for (a) cases MD1 and PD1 and (b) cases MD2 and PD2.

The symbols correspond to experimental data. [Color figure can be viewed in the online issue, which is available at wileyonlinelibrary.com.]

in the passive layer, the traveling time along this streamline from $i1$ to $j1$ is equal to the traveling time from $i2$ to $j2$, along the drum wall

$$t_{i1\to j1} = t_{i2\to j2} = \frac{\text{distance}_{i2\to j2}}{\text{velocity}_{i2\to j2}} \tag{12}$$

The velocity along the drum wall is related to the angular velocity (ω) of the rotating drum so that

$$t_{\text{pas}} = t_{i2\to j2} = \frac{R\alpha}{R\omega} = \frac{1}{\omega}\alpha \tag{13}$$

which means that the residence time t_{pas} along any streamline in the passive layer is proportional to α.

The residence time in the active layer has been modeled in the literature by Sturman et al.[50]

$$t_{\text{act}} = \frac{\pi}{\sqrt{\omega\dot{\gamma}}} \tag{14}$$

Here, another point of view is proposed and compared with Eq. 14. To do so, it is assumed that the glass beads travel along a straight line in this region (dashed line $j1 - i1$ in Figure 1). This assumption neglects the curvature at the beginning and end of this streamline where the particles flow rapidly in the transverse direction. The consequence is that it increases the particle residence time, especially for small angles α where higher curvature is found. The streamwise velocity profile u along a streamline in the active layer obeys Eq. 5. The residence time in the active layer is $t_{\text{act}} = 2\int_0^L \frac{dx}{u}$, which can be approximated by $2L/\bar{u}$, where $\bar{u} = \frac{1}{L}\int_0^L u dx = \frac{2}{3}u_{\text{act}}$. By combining these expressions, it follows that

$$t_{\text{act}} = \frac{3L}{u_{\max}\left(1+\frac{y+H}{\delta_\circ}\right)} \tag{15}$$

The value of L for a given streamline can be obtained from the location of the boundary between the active and passive layers, by setting $x = L$ in Eq. 6

$$L = \sqrt{\frac{y+\delta_\circ+H}{a}} \tag{16}$$

Substituting Eq. 16 and $u_{\max}$ from Eq. 4 into Eq. 15, and recalling that $a = \delta_\circ/L^{*2}$ yield

$$t_{\text{act}} = \frac{3\delta_\circ}{\omega L^*}\frac{1}{\sqrt{1+\frac{y+H}{\delta_\circ}}} \tag{17}$$

This equation shows that the residence time in the active layer should increase with an increase of the depth y. Introducing $\zeta = \frac{y+H}{\delta_\circ}$ and considering that in most of the reported data (as can be seen from Figure 7) $\zeta \in (-0.8, 0)$, $\frac{1}{\sqrt{1+\zeta}}$ can be approximated by its value at middle point $\zeta = -0.4$. Equation 17 then becomes

$$t_{\text{act}} = \frac{3.87\delta_\circ}{\omega L^*} \tag{18}$$

According to Eq. 18, the residence time in the active layer depends only on the operating conditions (ω) as well as the geometrical characteristics of the drum (L^*) and the thickness of the active layer $\delta_\circ$.

To asses the validity of Eqs. 13, 14, and 18, the residence times of the glass beads in the active and passive layers vs. the angle of the streamline are given in Figure 7. It can be readily seen that there are no significant differences between the monodisperse and polydisperse cases. One may notice that the residence time in the passive layer varies linearly when the angle of the streamlines increases, whereas it is constant in the active layer. Consequently, the total residence time (t_t, the summation of the residence times in both layers) also varies linearly. Moreover, there is a good agreement between the experimental data and what is expected from the short dashed lines (solid body rotation according to Eq. 13) in the passive layer, the dotted lines (Eqs. 14 and 18) in the active layer, and the solid lines (total residence time from the sum of Eqs. 13 + 14 or 13 + 18). Average values of the residence time in the active layer from Eqs. 14 and 18 are compared with those deduced from RPT data in Table 4. Note that these experimental data were obtained by averaging the residence times of many randomly selected streamlines in the active layer. A good agreement can be noticed in all cases between the measured and predicted values.

Table 4. Average Residence Time in the Active Layer

Case	Rotational Speed (RPM)	Experiment	t_{act} Eq. 14; (Measured $\delta_\circ$—Table 3)	t_{act} Eq. 18; (Measured $\delta_\circ$—Table 3)
MD1	5.4	1.47 ± 0.12	1.26	1.25
PD1	5.4	1.46 ± 0.12	1.39	1.54
MD2	11.6	0.87 ± 0.04	0.86	0.77
PD2	11.6	0.84 ± 0.06	0.95	0.80

All data are in second. The range indicated for the experimental data corresponds to the standard deviation.

Segregation

The difference in the size of the glass beads in the polydisperse cases (see Table 1) is large enough for radial segregation in the cylindrical drum to manifest itself in the first few drum rotations. To characterize the particle segregation, occupancy plots obtained from RPT data can be used. In Figure 8, the red and blue colors correspond to the higher and lower probabilities of occurrence of the tracer at a given position, respectively. Note that the blends of glass beads were mixed initially. The small particles end up in the central core of the bed, whereas the large particles concentrate mainly in the surrounding shell section. More precisely, 3-mm particles are present in the core, 4-mm particles are present everywhere in the granular bed but mainly in the inner layers, whereas large 5- and 6-mm particles surround the small particles.

To provide a more quantitative analysis, the occurrence probabilities of the different tracers along the middle line at $x = 0$ are presented in Figure 9 for the PD1 (5.4 RPM) and PD2 (11.6 RPM) cases. First, it can be readily noticed that the impact of the drum rotational speed is not significant. More precisely, it can be observed that, for both cases, the small 3-mm particles are located in the core of the granular bed, whereas the large 5- and 6-mm particles surround these small particles. Moreover, the 4-mm particles can be found everywhere in the granular bed, and it seems that they do not accumulate in the core region close to the material axis of rotation. This is contrary to the literature where it is always assumed that small particles are mainly present in the core.[6] Thus, in an operation where one or more species need to be distributed across the radial direction of the drum, inert granules of

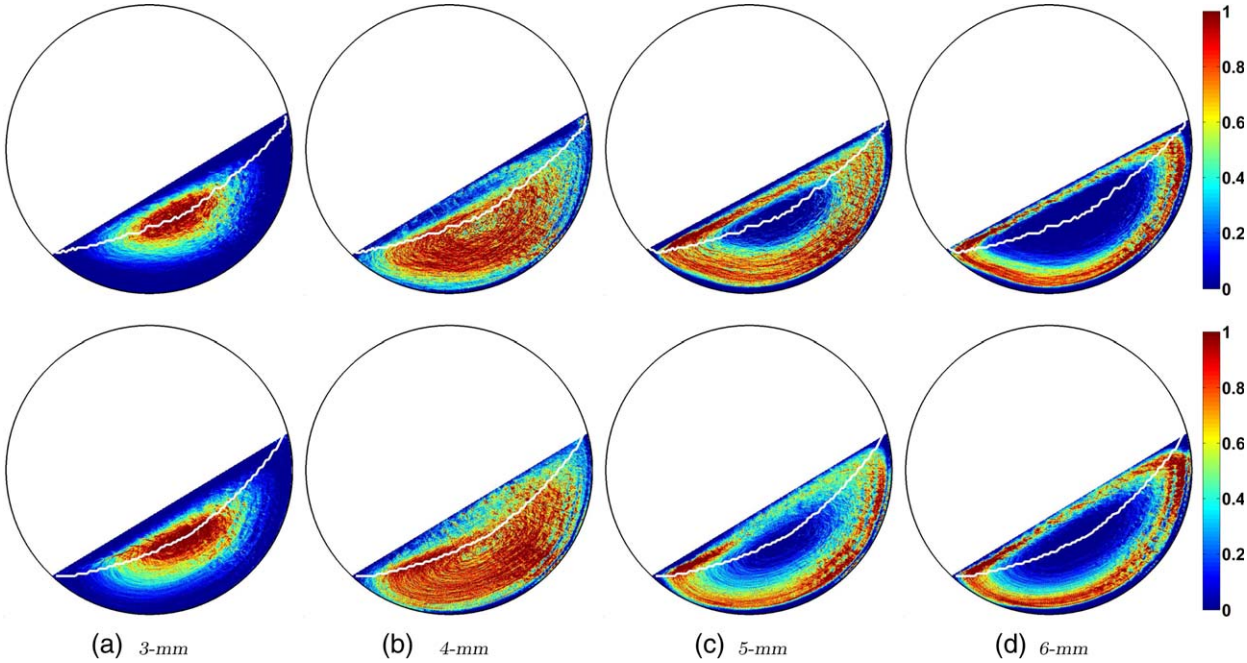

Figure 8. Occupancy plots for the different tracers in the polydisperse mixtures; the upper and lower plots refer to cases PD1 and PD2, respectively.

The white curve highlights the boundary between the passive and active layers on the basis of the turning point criterion. [Color figure can be viewed in the online issue, which is available at wileyonlinelibrary.com.]

different sizes could be added to the granular media to regulate the species concentrations along this direction.

As mentioned before, differences in the dynamic repose angle of the components of a mixture are believed to be the main reason for the occurrence of axial segregation and the formation of axial bands.[15,16] In our experiments, there were no measurable differences in the dynamic repose angle of the monodisperse and polydisperse mixtures (~27°), and the glass beads of different sizes did not form axial bands, even after around 2500 revolutions. Similar results for glass beads were reported by Zik et al.[10]

Axial dispersion

To be efficient, mixing must take place in both the axial and the radial directions of the cylindrical drum. The governing mechanisms are dispersion in the axial direction and a combination of convection and dispersion in the radial direction. As dispersion is slower than convection, tumbling blenders always suffer from weak axial mixing.[51] Therefore, the axial dispersion coefficient, D_{axial}, is a useful index to quantify the relative motion of the particles and thereby asses mixing efficiency in the axial direction.

Particles slowly drift along the drum axis of rotation, so that, in our experiments, they could only travel the full blender length a few times during 2500 revolutions. In particular, this indicates that the axial dispersion of the glass beads inside the drum was indeed very slow. It has been shown that the distribution of particle axial displacements is similar to a normal distribution.[18] The axial displacement distribution for the 3-mm tracer, measured for each cycle, is

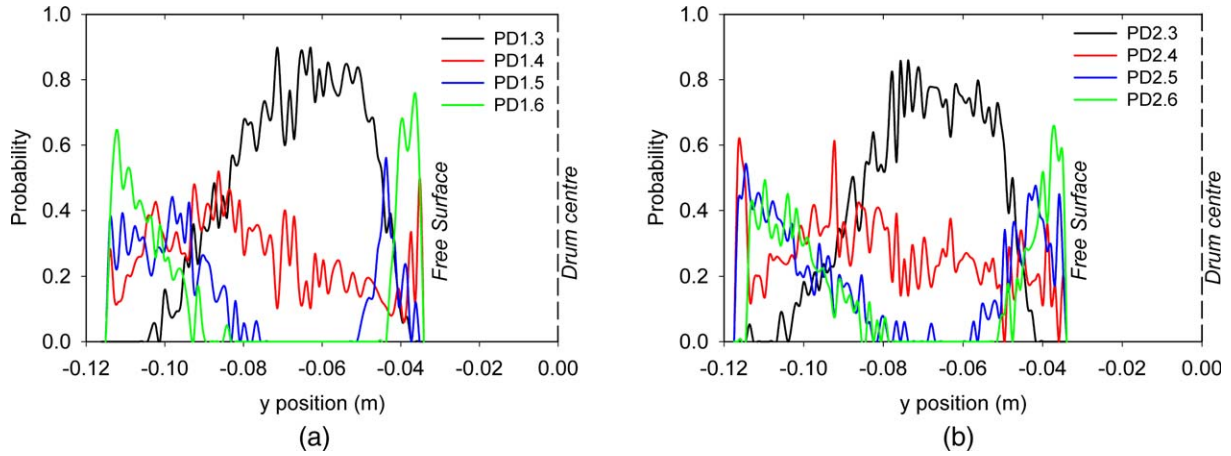

Figure 9. Probability of the occurrence of the different tracers along the middle line at $x = 0$; (a) case PD1 and (b) case PD2.

[Color figure can be viewed in the online issue, which is available at wileyonlinelibrary.com.]

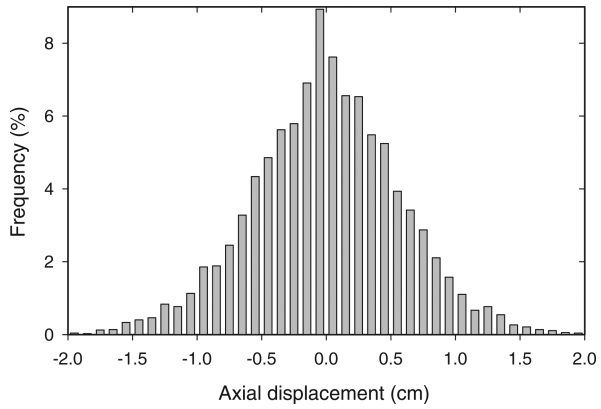

Figure 10. Typical axial displacement distribution for the 3-mm tracer in the monodisperse case MD2.

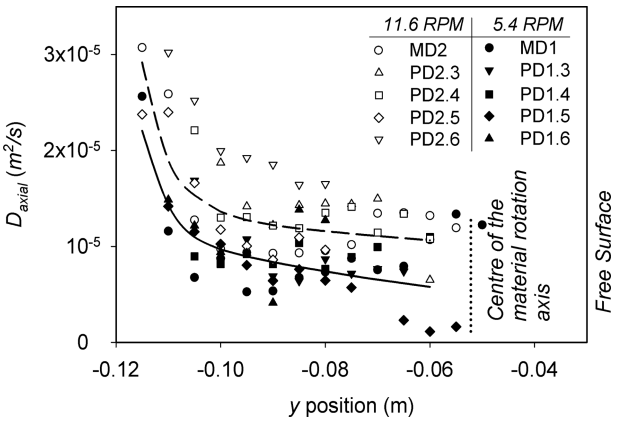

Figure 11. Variation of the axial dispersion coefficient along the line at $x = 0$ in the transverse plane of the drum.

given in Figure 10 for case MD2. The dispersion coefficient in the axial direction can be approximated by means of Einstein's law[52]

$$D_{\text{axial}} = \frac{\sum_i^n (\Delta z_i - \bar{\Delta} z_i)^2 / \Delta t_i}{2n} \tag{19}$$

where Δz_i is the axial displacement of the tracer during the ith cycle ($i = 1,\ldots,n$), Δt_i the time interval, and $\bar{\Delta z}$ the mean axial displacement, which should be 0 for a large number n of cycles.

D_{axial} corresponds to the variance of the measured displacements and is in fact the sum of two variances that come from the tracer displacement and the measurement error. Large time intervals generally lead to a high variance due to large displacements, whereas the variance related to the measurement error remains constant. The latter can then be made negligible by increasing the time interval. In this study, the residence time of granules along streamlines was chosen as the time interval, which guarantees that the measurement error does not alter significantly the dispersion coefficients, as discussed by Sherritt et al.[53]

D_{axial} is a function of the glass beads properties as well as the drum geometry and the operating conditions. Figure 11 shows the variation of the axial dispersion coefficient along the line $x = 0$ in the transverse plane of the drum. To obtain these results, this transverse plane has been divided into thin annuli, and an axial dispersion coefficient has been calculated in each section. The figure shows that the axial dispersion coefficient is nearly constant in the inner layers and slightly increases near the drum wall. This trend is shown with solid and dashed lines for the low and high rotational speeds, respectively. These lines were obtained by averaging the experimental data points in each rotational speed. These results are reasonable, as, in the layers close to the wall, the particles have more freedom to move axially because they eventually reach the free surface. Consequently, greater values of the axial dispersion coefficient are expected for the large particles that are in the outer layers. Rather similar results have been obtained by Ingram et al.[18] who showed an increase in axial dispersion with an increase of the particle size except for very large particles that ended up in the core of the bed. Values of D_{axial} for the different tracers are given in Table 5. First, these values are comparable to those reported in the literature. Ding et al.[31] obtained an axial dispersion coefficient of 3×10^{-6} m^2/s for 3-mm glass beads and a drum rotational speed of 9.6 RPM, whereas Sherritt et al.[53] reported values of the order of 10^{-5} m^2/s for rotational speeds of 5–25 RPM. Next, it can be noticed that D_{axial} is proportional to the drum rotational speed and that its value slightly increases with an increasing particle size.

Finally, Table 6 summarizes most of the findings of this work in the case of monodisperse and polydisperse systems of glass beads.

Concluding Remarks

In this work, the flow of monodisperse and polydisperse systems of glass beads were investigated inside a rotating cylindrical drum when operated in rolling mode. RPT, a powerful tool for characterizing the granular flow of opaque systems, was used to track a single radioactive tracer. ^{24}Na was used as the radioactive isotope, thanks to the presence of ^{23}Na in the glass beads. This resulted in a tracer with physical properties (size and density) identical to those of the nonradioactive glass beads. No significant differences were observed for the flow behavior of the monodisperse and polydisperse mixtures considered in this work. Note that different behaviors might be observed for large particle size ratios.[18] The following findings were obtained:

- There are only small differences between the velocity profiles and the active layer thicknesses of the monodisperse and polydisperse cases. This was confirmed by both experimental data and predictive models developed within the scope of this work;
- Small particles (3 mm) are present in the core section of the bed, whereas large particles (5 and 6 mm) surround them. Particles with an average size (4 mm) are

Table 5. Axial Dispersion Coefficient for the Different Experiments

		D_{axial} (m^2/s)	
Case	Tracer Size	5.4 RPM	11.6 RPM
Monodisperse	3 mm	8.3×10^{-6}	15×10^{-6}
Polydisperse	3 mm	7.0×10^{-6}	16×10^{-6}
	4 mm	9.2×10^{-6}	18×10^{-6}
	5 mm	10.9×10^{-6}	19×10^{-6}
	6 mm	12.2×10^{-6}	21×10^{-6}
Average value		9.5×10^{-6}	18×10^{-6}

Table 6. Summary of the Similarities and Differences Between the Flow Behavior of Monodisperse, Binary, and Polydisperse Systems of Particles

Issue	Polydisperse	Binary	Monodisperse
Segregation	Species distribute with respect to size in the transverse plane of the bed (see Figures 8 and 9)	A core/shell configuration is formed[8]	–
Dynamics of granules	Same velocity profiles in the streamwise and transverse directions (see Figure 4)		
Active layer thickness	Thickness of the active layer is around 30–40% of the granular bed, and it is thicker for the polydisperse case than for the monodisperse case (see Tables 2 and 3)		
Residence time	Residence times in passive and active layers can be obtained via $t_{\text{pas}} = \frac{1}{\omega}\alpha$ (Eq. 13) and $t_{\text{act}} = \frac{3.87\delta_\circ}{\omega L^*}$ (Eq. 18), respectively		
Axial dispersion coefficient	The axial dispersion coefficients are small $O(10^{-5})$ for the monodisperse and polydisperse cases and are proportional to the drum rotational speed and particle size (see Figure 11 and Table 5)		

found in the whole volume of the drum. This is true for the two rotational speeds considered (5.4 and 11.6 RPM);

- Particles do not have a lot of freedom when flowing in the axial direction, and the axial dispersion coefficient was found to be small in all cases. It was observed to increase slightly with an increase of radial position and to be proportional to the drum rotational speed;
- A model was developed to predict the residence time of granules in the active layer, and its validity was tested against RPT data. It was shown to predict correctly that the residence time is nearly constant in the active layer, whereas it varies linearly with an increase in the angle of the streamlines in the passive layer.

Acknowledgments

The authors thank the Research and Development Center of Ratiopharm operations (Mirabel, Québec) and the Natural Sciences and Engineering Research Council of Canada for financial support. They are grateful to Jean St-Pierre and Cornelia Chilian from the Institute of Nuclear Engineering for the activation of tracers and Majid Rasouli for helpful discussion regarding residence time.

Literature Cited

1. Jain N, Ottino JM, Lueptow RM. Regimes of segregation and mixing in combined size and density granular systems: an experimental study. *Granular Matter*. 2005;7(2–3):69–81.
2. So much more to know. *Science*. 2005;309(5731):78–102.
3. Meier S, Lueptow R, Ottino J. A dynamical systems approach to mixing and segregation of granular materials in tumblers. *Adv Phys*. 2007;56(5–6):757–827.
4. Mellmann J. The transverse motion of solids in rotating cylinders—forms of motion and transition behavior. *Powder Technol*. 2001; 118(3):251–270.
5. Cantelaube F, Bideau D. Radial segregation in a 2D drum: an experimental analysis. *Europhys Lett*. 1995;30(3):133–138.
6. Rapaport D. Radial and axial segregation of granular matter in a rotating cylinder: a simulation study. *Phys Rev E* 2007;75(3):31301.
7. Thomas N. Reverse and intermediate segregation of large beads in dry granular media. *Phys Rev E*. 2000;62(1):961–974.
8. Wightman C, Muzzio FJ. Mixing of granular material in a drum mixer undergoing rotational and rocking motions. II. Segregating particles. *Powder Technol*. 1998;98(2):125–134.
9. Aranson I, Tsimring L. Dynamics of axial separation in long rotating drums. *Phys Rev Lett*. 1999;82(23):4643–4646.
10. Zik O, Levine D, Lipson S, Shtrikman S, Stavans J. Rotationally induced segregation of granular materials. *Phys Rev Lett*. 1994; 73(5):644–647.
11. Huang A, Kuo H. A study of the three-dimensional particle size segregation structure in a rotating drum. *AIChE J*. 2012;58(4):1076–1083.
12. Taberlet N, Newey M, Richard P, Losert W. On axial segregation in a tumbler: an experimental and numerical study. *J Stat Mech: Theory Exp*. 2006;2006(07):P07013.
13. Alexander A, Muzzio FJ, Shinbrot T. Effects of scale and inertia on granular banding segregation. *Granular Matter*. 2004;5(4):171–175.
14. Choo K, Baker M, Molteno T, Morris S. Dynamics of granular segregation patterns in a long drum mixer. *Phys Rev E*. 1998; 58(5):6115–6123.
15. Hill K, Kakalios J. Reversible axial segregation of rotating granular media. *Phys Rev E*. 1995;52(4):4393–4400.
16. Bridgwater J, Foo W, Stephens DJ. Particle mixing and segregation in failure zones-theory and experiment. *Powder Technol*. 1985; 41(2):147–158.
17. Chen P, Ottino JM, Lueptow RM. Onset mechanism for granular axial band formation in rotating tumblers. *Phys Rev Lett*. 2010;104(18):188002.
18. Ingram A, Seville J, Parker D, Fan X, Forster R. Axial and radial dispersion in rolling mode rotating drums. *Powder Technol*. 2005;158(1–3):76–91.
19. Muzzio F, Robinson P, Wightman C, Dean B. Sampling practices in powder blending. *Int J Pharm*. 1997;26(2):153–178.
20. Muzzio FJ, Goodridge CL, Alexander A, Arratia P, Yang H, Sudah O, Mergen G. Sampling and characterization of pharmaceutical powders and granular blends. *Int J Pharm*. 2003;250(1):51–64.
21. Hawkesworth M, Parker D, Fowles P, Crilly J, Jefferies N, Jonkers G. Nonmedical applications of a positron camera. *Nucl Instrum Methods Phys Res Sect A*. 1991;310(1–2):423–434.
22. Parker D, Broadbent C, Fowles P, Hawkesworth M, Mcneil P. Positron emission particle tracking—a technique for studying flow within engineering equipment. *Nucl Instrum Methods Phys Res Sect A*. 1993;326(3):592–607.
23. Larachi F, Kennedy G, Chaouki J. A gamma ray detection system for 3-D particle tracking in multiphase reactors. *Nucl Instrum Methods Phys Res Sect A*. 1994;338(2–3):568–576.
24. Doucet J, Bertrand F, Chaouki J. An extended radioactive particle tracking method for systems with irregular moving boundaries. *Powder Technol*. 2008;181(2):195–204.
25. Beam GB, Wielopolski L, Gardner RP, Verghese K. Monte Carlo calculation of efficiencies of right-circular cylindrical NaI detectors for arbitrarily located point sources. *Nucl Instrum Methods*. 1978; 154(3):501–508.
26. Jain N, Ottino J, Lueptow R. Effect of interstitial fluid on a granular flowing layer. *J Fluid Mech*. 2004;508:23–44.
27. Nakagawa M, Altobelli S, Caprihan A, Fukushima E, Jeong EK. Non-invasive measurements of granular flows by magnetic resonance imaging. *Exp Fluids*. 1993;16(1):54–60.
28. Bonamy D, Daviaud F, Laurent L. Experimental study of granular surface flows via a fast camera: a continuous description. *Phys Fluids*. 2002;14(5):1666–1673.
29. Jain N, Ottino J, Lueptow R. An experimental study of the flowing granular layer in a rotating tumbler. *Phys Fluids*. 2002;14(2):572–582.
30. Khakhar D, McCarthy J, Ottino J. Radial segregation of granular mixtures in rotating cylinders. *Phys Fluids*. 1997;9(12):3600–3614.

31. Ding Y, Forster R, Seville J, Parker D. Segregation of granular flow in the transverse plane of a rolling mode rotating drum. *Int J Multiphase Flow*. 2002;28(4):635–663.
32. Mu J, Perlmutter DD. The mixing of granular solids in a rotary cylinder. *AIChE J*. 1980;26(6):928–934.
33. Kelbert F, Royere C. Lateral mixing and heat transfer in a rolling bed. *Int Chem Eng*. 1991;31(3):441–449.
34. Liu XY, Specht E. Predicting the fraction of the mixing zone of a rolling bed in rotary kilns. *Chem Eng Sci*. 2010;65(10):3059–3063.
35. Cheng NS, Zhou Q, Tan SK, Zhao K. Application of incomplete similarity theory for estimating maximum shear layer thickness of granular flows in rotating drums. *Chem Eng Sci*. 2011;66(12):2872–2878.
36. Ding Y, Seville J, Forster R, Parker D. Solids motion in rolling mode rotating drums operated at low to medium rotational speeds. *Chem Eng Sci*. 2001;56(5):1769–1780.
37. Ding Y, Forster R, Seville J, Parker D. Granular motion in rotating drums: bed turnover time and slumping-rolling transition. *Powder Technol*. 2002;124(1–2):18–27.
38. Liu XY, Specht E, Gonzalez O, Walzel P. Analytical solution for the rolling-mode granular motion in rotary kilns. *Chem Eng Process*. 2006;45(6):515–521.
39. Weir G, Krouse D, McGavin P. The maximum thickness of upper shear layers of granular materials in rotating cylinders. *Chem Eng Sci*. 2005;60(7):2027–2035.
40. Henein H, Brimacombe J, Watkinson A. Experimental study of transverse bed motion in rotary kilns. *Metall Trans B*. 1983;14 B(2):191–205.
41. Woodle GR, Munro JM. Particle motion and mixing in a rotary kiln. *Powder Technol*. 1993;76(3):241–245.
42. Boateng A, Barr P. Granular flow behaviour in the transverse plane of a partially filled rotating cylinder. *J Eng Appl Sci*. 1997;330:233–249.
43. Van Puyvelde D, Young B, Wilson M, Schmidt S. Modelling transverse segregation of particulate solids in a rolling drum. *Chem Eng Res Des*. 2000;78(4):643–650.
44. Orpe AV, Khakhar DV. Scaling relations for granular flow in quasi-two-dimensional rotating cylinders. *Phys Rev E*. 2001;64:031302.
45. Khakhar D, Orpe AV, Ottino J. Surface granular flows: two related examples. *Adv Complex Syst*. 2001;64(4):407–417.
46. Felix G, Falk V, D'Ortona U. Segregation of dry granular material in rotating drum: experimental study of the flowing zone thickness. *Powder Technol*. 2002;128(2–3):314–319.
47. Felix G, Falk V, D'Ortona U. Granular flows in a rotating drum: the scaling law between velocity and thickness of the flow. *Eur Phys J E*. 2007;22(1):25–31.
48. Boateng AA. Boundary layer modeling of granular flow in the transverse plane of a partially filled rotating cylinder. *Int J Multiphase Flow*. 1998;24(3):499–521.
49. Ottino J, Khakhar D. Scaling of granular flow processes: from surface flows to design rules. *AIChE J*. 2002;48(10):2157–2166.
50. Sturman R, Meier S, Ottino J, Wiggins S. Linked twist map formalism in two and three dimensions applied to mixing in tumbled granular flows. *J Fluid Mech*. 2008;602:129–174.
51. Lemieux M, Bertrand F, Chaouki J, Gosselin P. Comparative study of the mixing of free-flowing particles in a V-blender and a bin-blender. *Chem Eng Sci*. 2007;62(6):1783–1802.
52. Einstein A. Über die von der molekularkinetischen Theorie der Wrme geforderte Bewegung von in ruhenden Flüssigkeiten suspendierten Teilchen (On the movement of small particles suspended in a stationary liquid demanded by the molecular-kinetic theory of heat). *Ann Phys (Leipzig)*. 1905;322(8):549–560.
53. Sherritt R, Chaouki J, Mehrotra A, Behie L. Axial dispersion in the three-dimensional mixing of particles in a rotating drum reactor. *Chem Eng Sci*. 2003;58(2):401–415.

Manuscript received Jun. 22, 2012, and revision received Oct. 10, 2012